An intracavity frequency doubled H_2 Raman laser scheme for generating narrow-linewidth yellow radiation

Jonathan Tyler Green* and Leonardo Fallani

Laboratorio Europeo di Spettroscopie Nonlineari (LENS) and Dipartimento di Fisica ed Astronomia-Università di Firenze, Via Nello Carrara 1, 50019 Sesto Fiorentino, Italy
**Corresponding author: green@lens.unifi.it*

Received December 16, 2011; revised February 8, 2012; accepted February 8, 2012; posted February 8, 2012 (Doc. ID 160157); published April 30, 2012

We propose a cavity-based combined Raman and second harmonic generation scheme for generating hundreds of milliwatts of continuous-wave yellow radiation with a frequency linewidth suitable for spectroscopic applications. We suggest using H_2 gas as the Raman medium in an external Raman ring resonator with an intracavity frequency doubling crystal. Using gas rather than a crystal allows for single-mode, narrow-linewidth operation suitable for many spectroscopic applications. In a specific numerical example, we predict the generation of more than 200 mW of narrow-linewidth 583 nm light from an input of 1 W of 785 nm light, which could be obtained from a low cost tapered amplifier diode system. Finally, we suggest methods for improving the laser performance.

OCIS codes: 140.3550, 140.3560, 140.3515, 290.5910.

1. INTRODUCTION

One of the challenges facing scientists in a variety of fields is the generation of high-quality radiation at wavelengths out of the range of conventional laser sources. This demand is particularly important for frontier atomic physics experiments, where lasers are used to control and manipulate the internal as well as the external (motional) states of atoms. Highly developed diode laser and amplifier technologies based on such materials as InGaAs and GaAlAs operate in the near-infrared (NIR) and IR wavelength range required for cooling alkali atoms such as rubidium, cesium, and potassium and have been the foundation of many sophisticated atomic physics experiments. Ytterbium and erbium fiber doping technology has resulted in very high-quality fiber amplifiers and lasers near 1060 nm and 1550 nm that are seeing a great deal of use in atomic and optical physics laboratories as well. The use of frequency doubling schemes based on intracavity second harmonic generation (SHG) has also made high-power, high-quality continuous-wave (CW) radiation available over much of the violet to green spectrum.

Generation of midpower high-quality light in the yellow region of the visible spectrum remains challenging as it falls out of the range of common frequency doubled diodes and amplifiers. High-quality CW radiation in this regime would have many spectroscopic applications; for example, the $^1S_0 \rightarrow {}^3P_0$ clock transition in ytterbium is at 578 nm [1] and the 583 nm cooling transition of erbium [2] can be used for erbium trapping. Frequency doubled quantum dot lasers provide a means to produce narrow-linewidth radiation in this region suitable for many spectroscopic purposes [3], but, due to the lack of amplifiers at these quantum dot laser frequencies, the usable yellow output power is around the 10 mW level. Another route to generating CW yellow light is through exclusively $\chi^{(2)}$ nonlinear processes such as sum-frequency generation [4,5], which requires two sources that must be combined in an optical cavity, or a combination of sum-frequency and SHG [6]. Raman fiber amplifiers are now being used to generate high-quality yellow light as well, although these amplifiers are still quite expensive.

Other methods for producing light in this region use SHG together with stimulated Raman scattering (SRS), a $\chi^{(3)}$ process, inside an optical cavity [7]. These techniques have been quite successful in generating yellow light with CW powers near 3 W from all-solid-state configurations [8,9], and progress is being made in using the superior nonlinear and thermal properties of diamond [10] to produce CW Raman lasers as well [11]. These solid-state lasers produce high-power radiation and also are quite compact and sturdy, with typical cavity lengths of 2.5–5 cm. The current solid-state SHG + SRS CW lasers suffer from large intracavity losses due to scattering from the surfaces on the two to three crystals inside the cavity; this increases the Raman laser threshold to pump laser powers of 1.5 W or higher [9,12]. While solid-state Raman lasers show great potential for use in areas such as medicine and remote sensing, at this point they cannot be used in the field of precision spectroscopy. The primary reason for this is the multimode nature of the yellow output, which can be attributed mainly to the broad Raman linewidth of solid-state Raman media, which ranges from 1 to 6 cm^{-1}, while the typical resonator free spectral range is between 3 and 6 GHz. In one study of CW solid-state Raman lasers, this longitudinal mode competition resulted in output power fluctuations of 15% [13].

We would like to propose a SHG + SRS scheme that uses a diatomic gas as a Raman medium and could offer advantages over the solid-state schemes for a number of important applications by generating hundreds of milliwatts of single-mode tunable light with a linewidth suitable for spectroscopy.

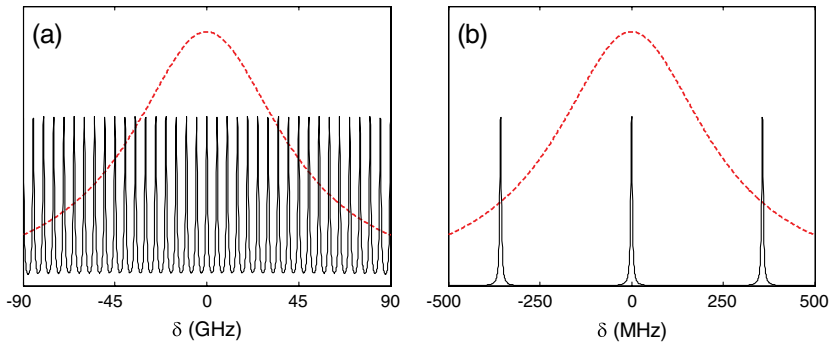

Fig. 1. (Color online) Longitudinal mode overlap with the Raman laser gain profile for an (a) Nd : $GdVO_4$ Raman laser with a 3 cm cavity length and (b) an H_2 Raman ring laser with an 84 cm cavity at a pressure of 10 atm. It is clear that the narrow Raman linewidth of H_2 will allow for single-mode operation, while the crystal-based laser will be multimode. δ is the two-photon detuning from the Raman resonance $(\nu_{\text{pump}}-\nu_{\text{Stokes}}-\nu_{\text{Raman}})$.

The Raman gain coefficient for Raman crystals is several times that of the Raman gas we consider here; however, a Raman gas has important properties that allow it to fill a niche that its solid-state counterparts cannot. The relatively narrow Raman linewidth, on the order of 500 MHz for H_2 and D_2 at 10 atm at room temperature, allows for single-mode operation and the capacity to carry out important spectroscopic tasks, such as locking to atomic resonances. Figure 1 compares the Raman laser gain curve (the Raman linewidth) with the longitudinal modes for the gaseous system considered in this paper and a typical crystal-based SRS + SHG laser based on Nd : $GdVO_4$ with a 3 cm cavity length. While the crystal-based laser has roughly 18 longitudinal modes within the Raman gain bandwidth, the gaseous laser considered here has two, which is quite suitable for narrow-linewidth, single-mode operation with a large continuous frequency tuning range. This scheme also has lower complexity and cost than sum-frequency generation schemes and commercial Raman amplification schemes, respectively.

Optical cavity-based SRS in diatomic gases has been the subject of much recent research. Carlsten and colleagues have laid the theoretical foundation for Raman gas-based CW lasers [14,15], and high-power Raman lasers in such systems have been constructed with H_2 or D_2 pressures ranging from 0.1 atm to 10 atm [16,17]. Cavity-based SRS with diatomic gas has also been proposed as a method for the construction of molecular modulators [18] for use in ultrashort pulse generation, and experimental progress has been made toward this goal as well [19,20].

2. PRINCIPLE OF OPERATION AND OUTLINE OF MODEL

The proposed scheme is depicted in Fig. 2. The principle of this SRS + SHG laser is to shift an input pump laser frequency down by the vibrational frequency of the molecules in the Raman medium through SRS; the downshifted beam, termed Stokes, is then frequency doubled by a nonlinear crystal inside the cavity. Each of the mirrors of the bowtie cavity are highly reflective at both the pump and the Stokes wavelengths. The pump is locked to the cavity and a resonant Stokes field begins from noise and builds up in the cavity. The intense Stokes field is then doubled in the nonlinear crystal and the second harmonic exits the cavity immediately. It is important to emphasize that the only frequency lock involved in this scheme is between the cavity and the pump laser; because the Stokes field begins from noise, the double resonance condition of the cavity is automatically fulfilled as long as the resonant Stokes frequency falls within the Raman linewidth. This reduces the system complexity as there is no need to lock two lasers to the cavity or tune the Stokes field with a dispersive gas. Tuning the pump frequency tunes the output yellow radiation frequency as well; for the system considered in the simulations below, we find that the continuous tuning range of the yellow output radiation should be roughly 1 GHz. This tuning flexibility will allow the yellow radiation to be locked to atomic resonances using standard diode laser feedback techniques.

The bowtie geometry of the cavity offers some important advantages over a two-mirror configuration. The unidirectional nature of the circulating fields ensures that the frequency doubled output of the nonlinear crystal all exits through one output coupler and there is no need for intracavity reflectors coated at the output wavelength [21]. The ring cavity configuration also reduces the effects of thermal lensing by the Raman medium [22]. The gas is heated due to the inelastic nature of Raman scattering, leading to an intensity dependent variation in the molecular density and, therefore, refractive index. This variation in the refractive index degrades the coupling efficiency of the pump and reduces

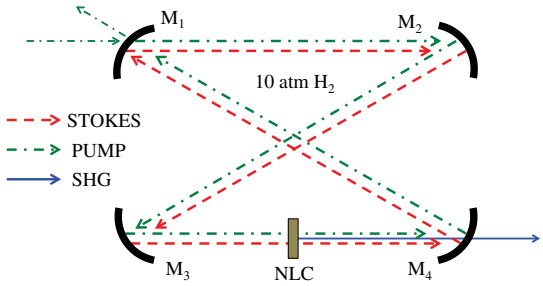

Fig. 2. (Color online) Basic schematic for the laser system. The mirrors of the bowtie cavity are highly reflective at both the pump and Stokes frequencies. For the example explored in this work, the cavity is completely immersed in 10 atm of H_2. The pump, Stokes, and SHG wavelengths are 785 nm, 1166 nm, and 583 nm, respectively, the curvature of all the mirrors is 15 cm, the round trip path length is 84 cm, and the nonlinear crystal (NLC) is taken to have the properties of MgO:PPLN with a length of 6 mm.

the efficiency of the Raman laser; this has been modeled for two-mirror standing wave H_2 Raman lasers [15]. The ring configuration increases the mode volume in the gas and distributes the energy over a larger number of molecules, greatly reducing the amount of thermal lensing. In this work we take our intracavity circulating Stokes power to be comparable to powers already achieved and shown not to suffer significantly from thermal lensing [22], so we expect similar behavior and that this model will be a good approximation to operation with thermal effects included.

High finesse resonant cavities in a ring configuration are known to suffer from backwards propagating modes that can hinder performance; ring cavity Raman gas lasers are not observed to suffer from these effects near the peak of the Raman gain [22]. The Doppler Raman linewidth for the backward propagating Stokes mode is significantly larger than that of the forward:

$$(\Delta\nu_{\text{Doppler}})_{\text{backward}} = (\nu_p + \nu_s)\sqrt{\frac{8\kappa T\,\log(2)}{mc^2}}, \tag{1}$$

$$(\Delta\nu_{\text{Doppler}})_{\text{forward}} = (\nu_p - \nu_s)\sqrt{\frac{8\kappa T\,\log(2)}{mc^2}}, \tag{2}$$

which results in a much lower peak Raman gain for a backwards propagating Stokes mode [23,24]. This asymmetry suppresses backward or bistable operation. One drawback of using a bowtie configuration is the lower achievable cavity finesse. In the system we explore in this paper, cavity losses are dominated by scattering from the nonlinear crystal so the detrimental effect of adding more mirrors to the cavity is less significant.

The most commonly used molecules for Raman gas lasers are H_2 and D_2 due to their large fractional population in the lowest ro-vibrational states and their large Raman shifting frequencies; the vibrational Raman transition in H_2, for example, has a frequency of 4155 cm^{-1}, or 125 THz. Stokes field gain in a nonlinear medium is characterized by the material Raman gain coefficient, α, as follows:

$$\frac{\mathrm{d}I_s}{\mathrm{d}z} = \alpha I_p(r,z) I_s(r,z), \tag{3}$$

where the indices p and s correspond to the pump and Stokes fields, respectively. The plane wave gain coefficient, α, can be calculated following the formalism of Harris and Sokolov [25] using tabulated oscillator strengths of the Lyman and Werner bands of H_2 or D_2 [26], or it can be taken from previous experimental measurements [27,28]. With α, we can characterize the Stokes power gain for a traveling Stokes wave within the cavity. A four-mirror optical cavity with four curved mirrors, in general, has four intracavity waists. One must account for this by calculating a gain for all four of the focal regions in cavity and taking the total cavity gain to be a weighted average of them. For clarity, in this work we make an approximation that the distance between each of the mirrors is $l/4$, where l is the total cavity length, and that each mirror has the same radius of curvature, which gives the same waist in each focal region. The pump and Stokes waves are both confined to the same cavity and have the same confocal parameter, $b = 2\pi w^2/\lambda$. To describe the Stokes gain in the cavity, we integrate Eq. (3) over a distance $l/4$ [15]. The pump and Stokes complex field amplitudes are described by [29]

$$E_{p(s)}(r,z) = \frac{E_{0;p(s)}}{1 + i(2\,z/b)} \exp\left(\frac{-r^2}{w_{p(s)}^2(1 + i(2\,z/b))}\right), \tag{4}$$

and the complex field amplitudes are related to the intensity as $I_i(r,z) = 1/(2\eta)|E_i(r,z)|^2$. In Eq. (4), $E_{0;p(s)}$ corresponds to the peak electric field for the pump (Stokes) beam. For the symmetric cavity considered here, the Raman gain contribution to the time evolution of the Stokes wave, neglecting thermal effects, is given by

$$\frac{\mathrm{d}P_s}{\mathrm{d}t} = \frac{16\alpha c}{l(\lambda_p + \lambda_s)} \tan^{-1}\left(\frac{l}{4\,b}\right) P_p P_s \tag{5}$$

$$\equiv G P_p P_s. \tag{6}$$

The optical cavity has mirrors that can be described in terms of reflectivity (R), transmissivity (T), and scattering/absorption (A) in the standard fashion: $1 = R + T + A$. Another very significant source of loss is the scattering from the nonlinear SHG crystal in the cavity characterized by κ, where κ is the transmission through crystal. The round trip loss coefficient, following the convention of Brasseur *et al.*, is then [14]

$$L_{p(s)} = \frac{c}{l} \ln\left(\sqrt{R_{1\,p(s)} R_{2\,p(s)} R_{3\,p(s)} R_{4\,p(s)} \kappa_{p(s)}}\right). \tag{7}$$

This allows us to write the full round trip differential equation through the Raman medium:

$$\frac{\mathrm{d}P_p}{\mathrm{d}t} = 2L_p P_p - \frac{\omega_p}{\omega_s} G P_s P_p + \frac{2\,c}{l}\sqrt{T_{1\,p} P_{p,\text{in}} P_p}, \tag{8}$$

$$\frac{\mathrm{d}P_s}{\mathrm{d}t} = 2L_s P_s + G P_p P_s. \tag{9}$$

We note that integration of Eqs. (8) and (9) alone converge to the steady state values found in Roos *et al.* [22]. Equations (8) and (9) describe the temporal evolution of the beams through the gas-filled cavity accounting for the spatial overlap of the pump and Stokes beams. The length of the frequency doubling crystal is comparatively small and located at the waist of the intracavity fields, so a plane wave approach to estimating the SHG is sufficient. To do this we propagate the fields over one cavity round trip through the Raman medium using Eqs. (8) and (9) and then use the plane wave spatial differential equations (10) and (11) to calculate the SHG power and the Stokes field loss per round trip [30], assuming perfect phase matching.

$$\frac{\mathrm{d}E_s}{\mathrm{d}z} = i\frac{2 d_{\text{eff}} \omega_s^2}{k_s c^2} E_{\text{shg}} E_s^*, \tag{10}$$

$$\frac{dE_{shg}}{dz} = i\frac{d_{eff}\omega_{shg}^2}{k_{shg}c^2}E_s^2. \quad (11)$$

The Stokes field input to the nonlinear crystal used in Eqs. (10) and (11) is the average field corresponding to the circulating Stokes power focused to the Stokes spot size at the nonlinear crystal, which is determined by the cavity geometry. The generated second harmonic field exits the cavity through the output coupler, which is not reflective at the second harmonic wavelength.

3. NUMERICAL EXAMPLE

To illustrate the expected performance of this scheme, we consider the generation of 583 nm light, the wavelength of an Erbium cooling transition, from a pump at 785 nm. In this simulation we choose experimental parameters such as intracavity powers, cavity finesse, etc. to be similar to those in previous experiments with gaseous Raman lasers where the formalism laid out above has been demonstrated to be very effective in describing Raman laser operation. The Raman system in this example is the vibrational Raman transition in H_2, which has a transition frequency of 4155 cm^{-1} (125 THz). We take α to be 1.5 cm/GW [28] and the Raman linewidth to be 500 MHz [31], at room temperature and a pressure of 10 atm, based on previous measurements.

The layout of the system considered in this example is shown in Fig. 2. The system geometry and mirror curvature are chosen to give a cavity mode with four approximately equal intracavity waists; this gives the cavity a single confocal parameter, b, for the whole length of the cavity, which is 84 cm. The radii of curvature for all of the concave mirrors is 15 cm, which gives cavity waists of 130 μm for the pump and 160 μm for the Stokes beam. By using four curved mirrors in the bowtie cavity the circulating waves remain tightly focused for a full round trip of the cavity, which increases the efficiency of the Raman process. All the mirrors are 99.98% reflective at the Stokes wavelength and mirrors 2–4 are 99.98% reflective at the pump wavelength, while the input coupler (mirror 1) is impedance matched to the cavity, taking into account scattering and conversion losses of the pump, and has a reflectivity of 99.1%. Scattering losses from the mirrors are assumed to be 100 ppm, but the main source of cavity loss is the crystal, which is taken to cause 0.4% loss (0.2% per crystal face) on the pump and Stokes power per round trip.

The Raman linewidth for 10 atm of H_2 at room temperature is 500 MHz, and the free spectral range of the cavity is 360 MHz. Because the cavity resonances are on the order of the Raman gain bandwidth, this system is well suited for single-mode operation; by choosing a shorter cavity length and tighter intracavity focusing, the number of longitudinal modes overlapping the Raman linewidth can be reduced further. The solid-state lasers, due to their broad Raman linewidths, as described above, have considerably more longitudinal modes overlapping the Raman gain bandwidth, which leads to multimode operation and mode competition. The large spread of longitudinal modes relative to the Raman linewidth allows for more than 1 GHz of continuous tuning for the system considered here, which is quite suitable for spectroscopic applications such as locking to atomic resonances.

The nonlinear crystal is taken to have the properties of periodically poled MgO : $LiNbO_3$ crystal with a length of 6 mm, which is positioned at one of the waists of the cavity. In the calculation, perfect phase matching of the 1166 nm Stokes field and the 583 nm SHG field is assumed, and the effect of the periodic poling is described by a nonlinear crystal coefficient $d_{eff} = \frac{2}{\pi}d_{33}$, which is 17 pm/V.

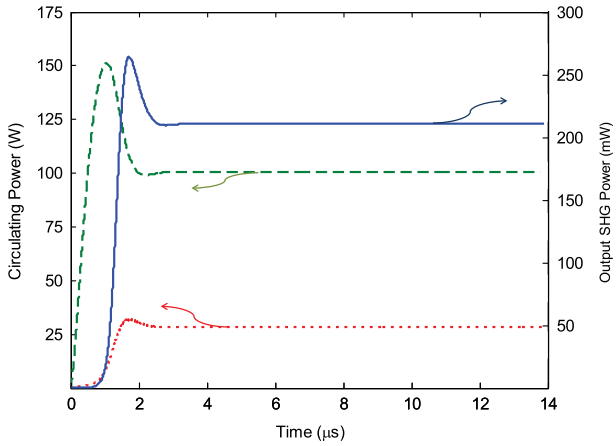

Fig. 3. (Color online) Temporal evolution of circulating pump and Stokes powers and output SHG power. Pump (785 nm), green dashed line; Stokes (1166 nm), red dotted line; output (583 nm), blue solid line. The arrows indicate the appropriate axis for each curve. The numerical simulations of this system predict a steady state value of 211 mW of 583 nm output power for 1 W of input 785 nm light.

The results of the simulation with these parameters is shown in Fig. 3. As the pump laser builds in the cavity, the Stokes field (at 1166 nm) reaches its threshold value and begins to lase. The Stokes power increases to the point that all excess 1166 nm Stokes photons are converted into 583 nm second harmonic photons that exit the cavity with a steady state power of 211 mW for 1 W of input power at 785 nm. We choose to use 1 W of input power, as it corresponds to 50% of the output of commercially available 2 W tapered amplifiers at this wavelength.

We expect the linewidth of the output radiation to be determined primarily by the mechanical stability of the cavity and not any intrinsic properties of the Raman process. A linewidth of 8 kHz was observed for a Raman laser [14] with intracavity parameters very similar to those considered here. Because the parameters associated with the Raman process are roughly the same, such as circulating Stokes power, we can also expect a linewidth in the tens of kHz; the linewidth of the output 583 nm radiation should be approximately twice the linewidth of the Stokes field, but we can still expect it to be less than 100 kHz. Beyond citing a measured linewidth with similar experimental parameters to those modeled here, it is quite difficult to confidently predict a laser linewidth, as it depends so heavily on the specific cavity design, but it is important to note that the Raman process itself is not the limiting factor in this respect; a well-designed and well-isolated optical cavity is predicted to achieve Stokes linewidths even in the sub-kHz regime [14].

4. DISCUSSION AND CONCLUSION

The balance between the efficiency of the SRS and SHG processes in these types of lasers is emphasized in [7]; an imbalance of SRS and SHG efficiencies can either result in inefficient conversion of the circulating Stokes field or can

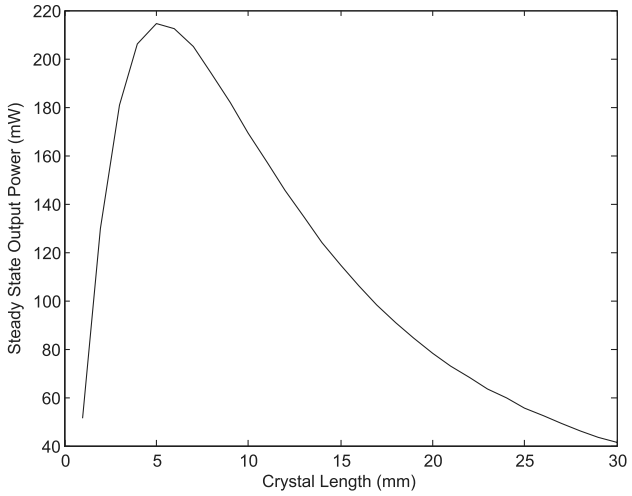

Fig. 4. Relationship between steady state Stokes power and nonlinear crystal length at 1 W on input pump power. As the strength of the SHG process is increased by increasing the crystal length in the simulation, the overall output power reaches a maximum value where the SHG and SRS processes balance. Above this point, the depletion of the Stokes beam via SHG reduces the Raman efficiency, causing the final output SHG power to drop.

prevent the Stokes field from building to an appreciable power in the cavity. Figure 4 illustrates this balance, showing a clear decrease in the overall NIR to yellow conversion past an optimum SHG crystal length. The efficiency of each of these processes is determined in part by the spot sizes on the doubling crystal and the beam size in the Raman medium; these parameters can be controlled by cavity geometry, so by adjusting the dimensions of the cavity and the mirror radii of curvature, one can tune the relative efficiencies of each of these processes.

One important practical consideration in designing the high finesse cavity is the bandwidth of the reflective coatings. In our example, high reflectivities were required at both the pump and vibrational Stokes wavelengths. Raman transitions can also be made between rotational levels; in H_2, for example, the $|\nu = 0, J = 1\rangle \rightarrow |\nu = 0, J = 3\rangle$ rotational Raman transition has a frequency of 17.6 THz. If the mirrors are highly reflective at the rotational Stokes wavelength, the laser may pump the rotational Stokes beam rather than the desired vibrational wavelength or the laser could suffer from competition between these modes [32]. This should be considered when choosing the bandwidth of the cavity mirror coatings.

In this simulation, the 785 nm input power is taken to be 1W, which is well within the range of most tapered amplifier-based diode laser systems. The 583 nm output power and efficiency would be increased by increasing the 785 nm input power by, for example, adding the output of two tapered amplifiers using the same seed in the optical cavity [33]. Such methods, while adding complexity to the scheme, could be worth the effort as an input pump power of 2 W for all the same cavity parameters would yield roughly 600 mW of 583 nm light.

The most straightforward way to improve the output power of this scheme would be to minimize the losses in the doubling crystal. The crystal losses assumed in this paper are typical of low cost antireflection (AR) coatings and are the main factor limiting the efficiency of the output radiation. Even reducing the scattering losses to 0.1% per surface from 0.2%, assumed in this paper, would increase the 583 nm output power to 370 mW, for the parameters considered above. Such powers and the expected sub 100 kHz linewidth could be suitable for more demanding spectroscopic applications such as atom trapping.

Finally, one should consider the material used to construct the gas container depending on the purity and pressure of the H_2. High strength steel, for example, is quite susceptible to hydrogen embrittlement. Depending on the design of the cavity, other materials, such as aluminum, that are much less susceptible to hydrogen embrittlement could be considered as well. For low pressures on the order of 10 atm, we don't expect hydrogen embrittlement in standard stainless steel to be an issue.

We have proposed a CW cavity-based SRS + SHG scheme that uses common laser diodes and tapered amplifiers to produce high-power, single-mode yellow light with a linewidth suitable for spectroscopic applications. By using a gas as the Raman medium, this laser is able to produce radiation much more suitable for spectroscopic purposes than solid-state Raman lasers, and the cost of this system would be much lower than other methods described above. We predict that more than 200 mW of yellow light can be produced from common 780 nm diode laser systems and typical AR coatings on the frequency doubling crystal. While suggesting methods for significantly improving the performance of the laser, our discussion has focused on using common and relatively low cost components and minimizing the system's complexity.

ACKNOWLEDGMENTS

We would like to thank Deniz Yavuz, Pablo Cancio Pastor, Francesco Marin, Jacopo Catani, Florian Schäfer, Guido Pagano, Francesca Ferlaino, Kiyotaka Aikawa, Roberto Bini, and Massimo Inguscio for very useful discussions. We acknowledge financial support from EU FP7 AQUTE, EU FP7 NAMEQUAM, and IIT ENCORE projects.

REFERENCES

1. S. G. Porsev, A. Derevianko, and E. N. Forston, "Possibility of an optical clock using the $6^1S_0 \rightarrow {}^3P_0$ transition in ^{171,173}Yb atoms held in an optical lattice," Phys. Rev. A **69**, 021403(R) (2004).
2. H. Y. Ban, M. Jacka, J. L. Hanssen, J. Reader, and J. J. McClelland, "Laser cooling transitions in atomic erbium," Opt. Express **13**, 3185–3195 (2005).
3. W. K. Lee, C. Y. Park, D. H. Yu, S. E. Park, S. B. Lee, and T. Y. Kwon, "Generation of 578-nm yellow light over 10 mW by second harmonic generation of an 1156-nm external-cavity diode laser," Opt. Express **19**, 17453–17461 (2011).
4. E. Mimoun, L. D. Sarlo, J. J. Zondy, J. Dalibard, and F. Gerbier, "Sum-frequency generation of 589 nm light with near-unit efficiency," Opt. Express **16**, 18684–18691 (2008).
5. Y. F. Chen, S. W. Tsai, S. C. Wang, Y. C. Huang, T. C. Lin, and B. C. Wong, "Efficient generation of continuous-wave yellow light by single-pass sum-frequency mixing of a diode-pumped Nd : YVO_4 dual-wavelength laser with periodically poled lithium niobate," Opt. Lett. **27**, 1809–1811 (2002).
6. G. Ferrari, "Generating green to red light with semiconductor lasers," Opt. Express **15**, 1672–1678 (2007).
7. K. Koch, G. T. Moore, and M. E. Dearborn, "Raman oscillation with intra-cavity second harmonic generation," IEEE J. Quantum Electron. **33**, 1743–1748 (1997).
8. H. Yu, Z. Li, A. J. Lee, J. Li, H. Zhang, J. Wang, H. Pask, J. Piper, and M. Jiang, "A continuous wave $SrMoO_4$ Raman laser," Opt. Lett. **36**, 579–581 (2011).

9. A. J. Lee, H. Pask, J. A. Piper, H. Zhang, and J. Wang, "An intracavity, frequency-doubled $BaWO_4$ Raman laser generating multi-watt continuous-wave, yellow emission," Opt. Express **18**, 5984–5992 (2010).
10. R. P. Mildren, "The outlook for diamond in Raman laser applications," Mater. Res. Soc. Symp. Proc. **1203**, 1203-J13-01 (2009).
11. W. Lubeigt, G. M. Bonner, J. E. Hastie, M. D. Dawson, D. Burns, and A. J. Kemp, "Continuous-wave diamond Raman laser," Opt. Lett. **35**, 2994–2996 (2010).
12. P. Dekker, H. M. Pask, D. J. Spence, and J. A. Piper, "Continuous-wave, intra-cavity doubled, self-Raman laser operation in $Nd:GdVO_4$ at 586.5 nm," Opt. Express **15**, 7038–7046 (2007).
13. A. J. Lee, H. M. Pask, T. Omatsu, P. Dekker, and J. A. Piper, "All solid-state continuous-wave yellow laser based on intra-cavity frequency-doubled self-Raman laser action," Appl. Phys. B **88**, 539–544 (2007).
14. J. K. Brasseur, P. A. Roos, K. S. Repasky, and J. L. Carlsten, "Characterization of a continuous-wave Raman laser in H_2," J. Opt. Soc. Am. B **16**, 1305–1312 (1999).
15. J. C. Bienfang, W. Rudolph, P. A. Roos, L. S. Meng, and J. L. Carlsten, "Steady-state thermo-optic model of a continuous-wave Raman laser," J. Opt. Soc. Am. B **19**, 1318–1325 (2002).
16. J. K. Brasseur, R. F. Teehan, P. A. Roos, B. Soucy, D. K. Neumann, and J. L. Carlsten, "High-power deuterium Raman laser at 632 nm," J. Opt. Soc. Am. B **43**, 1162–1166 (2004).
17. J. T. Green, D. E. Sikes, and D. D. Yavuz, "Continuous-wave high-power rotational Raman generation in molecular deuterium," Opt. Lett. **34**, 2563–2565 (2009).
18. D. D. Yavuz, "High-frequency modulation of continuous-wave laser beams by maximally coherent molecules," Phys. Rev. A **76**, 011805(R) (2007).
19. J. T. Green, J. J. Weber, and D. D. Yavuz, "Continuous-wave light modulation at molecular frequencies," Phys. Rev. A **82**, 011805 (2010).
20. J. J. Weber, J. T. Green, and D. D. Yavuz, "17 THz continuous-wave optical modulator," Phys. Rev. A **85**, 013805 (2012).
21. A. J. Lee, D. J. Spence, J. A. Piper, and H. M. Pask, "A wavelength-versatile, continuous-wave self-Raman solid-state laser operating in the visible," Opt. Express **18**, 20013–20018 (2010).
22. P. A. Roos, L. S. Meng, and J. L. Carlsten, "Doppler-induced unidirectional operation of a continuous-wave Raman ring laser in H_2," Appl. Opt. **42**, 5517–5521 (2003).
23. P. Lallemand, P. Simova, and G. Bret, "Pressure-induced line shift and collisional narrowing in hydrogen gas determined by stimulated Raman emission," Phys. Rev. Lett. **17**, 1239–1241 (1966).
24. N. Bloembergen, "The stimulated Raman effect," Am. J. Phys. **35**, 989–1022 (1967).
25. S. E. Harris and A. V. Sokolov, "Broadband spectral generation with refractive index control," Phys. Rev. A **55**, R4019–R4022 (1997).
26. A. C. Allison and A. Dalgarno, "Band oscillator strengths and transition probabilities for the Lyman and Werner systems of H_2, HD, and D_2," At. Data **1**, 289–304 (1969).
27. J. J. Ottusch and D. A. Rockwell, "Measurements of Raman gain coefficients in hydrogen, deuterium, and methane," IEEE J. Quantum Electron. **24**, 2076–2080 (1988).
28. W. K. Bischel and M. J. Dryer, "Wavelength dependence of the absolute Raman gain coefficient for the Q(1) transition in H_2," J. Opt. Soc. Am. B **3**, 677–682 (1986).
29. G. D. Boyd, W. D. Johnston, and I. P. Kaminow, "Optimization of the stimulated Raman scattering threshold," IEEE J. Quantum Electron. **5**, 203–206 (1969).
30. R. W. Boyd, *Nonlinear Optics*, 3rd ed. (Academic, 2008).
31. W. K. Bischel and M. J. Dryer, "Temperature dependence of the Raman linewidth and line shift for the Q(1) and Q(0) transitions in normal and para-H_2," Phys. Rev. A **33**, 3113–3123 (1986).
32. J. T. Green, J. J. Weber, and D. D. Yavuz, "Continuous-wave, multiple-order rotational Raman generation in molecular deuterium," Opt. Lett. **36**, 897–899 (2011).
33. G. Ferrari, J. Catani, L. Fallani, G. Giusfredi, G. Schettino, F. Schäfer, and P. C. Pastor, "Coherent addition of laser beams in resonant passive optical cavities," Opt. Lett. **35**, 3105–3107 (2010).